

PPPL-5278

Effect of progressively increasing lithium conditioning on edge transport and stability in high triangularity NSTX H-modes

R. Maingia, J.M. Canik^b, R.E. Bella, D.P. Boylec, A. Dialloa, R. Kaitaa, S.M. Kayea, B.P. LeBlanca, S.A. Sabbaghd, F. Scottie, V.A. Soukhanovskiie, and the NSTX team

August 2016



Prepared for the U.S. Department of Energy under Contract DE-AC02-09CH11466.

Princeton Plasma Physics Laboratory

Report Disclaimers

Full Legal Disclaimer

This report was prepared as an account of work sponsored by an agency of the United States Government. Neither the United States Government nor any agency thereof, nor any of their employees, nor any of their contractors, subcontractors or their employees, makes any warranty, express or implied, or assumes any legal liability or responsibility for the accuracy, completeness, or any third party's use or the results of such use of any information, apparatus, product, or process disclosed, or represents that its use would not infringe privately owned rights. Reference herein to any specific commercial product, process, or service by trade name, trademark, manufacturer, or otherwise, does not necessarily constitute or imply its endorsement, recommendation, or favoring by the United States Government or any agency thereof or its contractors or subcontractors. The views and opinions of authors expressed herein do not necessarily state or reflect those of the United States Government or any agency thereof.

Trademark Disclaimer

Reference herein to any specific commercial product, process, or service by trade name, trademark, manufacturer, or otherwise, does not necessarily constitute or imply its endorsement, recommendation, or favoring by the United States Government or any agency thereof or its contractors or subcontractors.

PPPL Report Availability

Princeton Plasma Physics Laboratory:

<http://www.pppl.gov/techreports.cfm>

Office of Scientific and Technical Information (OSTI):

<http://www.osti.gov/scitech/>

Related Links:

[U.S. Department of Energy](#)

[U.S. Department of Energy Office of Science](#)

[U.S. Department of Energy Office of Fusion Energy Sciences](#)

Effect of progressively increasing lithium conditioning on edge transport and stability in high triangularity NSTX H-modes

R. Maingi^a, J.M. Canik^b, R.E. Bell^a, D.P. Boyle^c, A. Diallo^a, R. Kaita^a, S.M. Kaye^a, B.P. LeBlanc^a, S.A. Sabbagh^d, F. Scotti^e, V.A. Soukhanovskii^e, and the NSTX team

^a Princeton Plasma Physics Laboratory, 100 Stellarator Road, Princeton, NJ 08543 USA

^b Oak Ridge National Laboratory, Oak Ridge, TN, USA

^c Princeton University, Princeton, NJ, USA

^d Columbia University, New York, NY, USA

^e Lawrence Livermore National Laboratory, Livermore, CA USA

A sequence of H-mode discharges with increasing levels of pre-discharge lithium evaporation ('dose') was conducted in high triangularity and elongation boundary shape in NSTX. Energy confinement increased, and recycling decreased with increasing lithium dose, similar to a previous lithium dose scan in medium triangularity and elongation plasmas. Data-constrained SOLPS interpretive modeling quantified the edge transport change: the electron particle diffusivity decreased by 10-30x. The electron thermal diffusivity decreased by 4x just inside the top of the pedestal, but increased by up to 5x very near the separatrix. These results provide a baseline expectation for lithium benefits in NSTX-U, which is optimized for a boundary shape similar to the one in this experiment.

PACS: 52.40.Hf, 52.25.-b, 52.30.-q, 52.55.-s

Keywords: NSTX, Lithium, Recycling, Pedestal, Energy Confinement

Corresponding Author Address: PPPL, 100 Stellarator Road, Princeton NJ 08543

Corresponding Author Email: rmaingi@pppl.gov

I. Introduction and Background

Lithium has been applied to plasma-facing components (PFCs) in fusion devices to improve performance with a number of delivery techniques. In addition to evaporation of metallic lithium discussed below, lithium pellets were injected in TFTR¹, DIII-D², and NSTX³, with modest to moderate short-term performance enhancement. Lithium was also used via a laser-based aerosol delivery system, which improved the $n\tau T$ triple product by more than a factor of 50 in TFTR⁴. In addition, lithium powder was delivered as an aerosol⁵ to improve performance in DIII-D⁶ and EAST⁷. Also, lithium granules were injected into EAST⁸ and DIII-D⁹, to ameliorate ELM size by increasing the natural ELM frequency. Finally liquid lithium was used in a static liquid lithium divertor configuration in NSTX¹⁰, a liquid lithium limiter in FTU¹¹, as a liquid on heated walls in LTX^{12, 13}, and as a flowing liquid lithium limiter in HT-7¹⁴ and EAST¹⁵. A recent review provides additional details¹⁶.

Lithium was evaporated via ovens into TJ-II¹⁷ and NSTX¹⁸⁻²⁰. In NSTX, recycling was reduced and confinement was improved; also ELMs were eliminated^{21, 22}, owing to an inward shift of the electron density profile relative to the electron temperature profile very close to the separatrix, which stabilized peeling-ballooning modes^{23, 24}. The magnitude of the increase in energy confinement in NSTX increased with the pre-discharge lithium evaporation ‘dose’^{25, 26}. In addition the density and pressure profile steep gradient regions shifted progressively away from the separatrix with increasing dose. Interpretive simulations with the SOLPS code indicated that the recycling coefficient at the divertor target dropped with increasing lithium evaporation, from ~

$R=0.99$ to $\sim R=0.85-0.90$ during this scan, and the core fueling rate dropped by 40-60%²⁷,²⁸. The required cross-field electron particle diffusivity D_e and electron thermal diffusivity χ_e increased modestly in the last 5% of normalized poloidal flux ψ_N near the separatrix, but decreased inside of that region, consistent with the observed steeper gradients and improved confinement²⁹.

The NSTX experiments and analysis mentioned in the last paragraph were performed in a moderate triangularity $\delta \sim 0.45$, elongation $\kappa \sim 1.8$ boundary shape, and then repeated in a high triangularity $\delta \sim 0.65$, elongation $\kappa \sim 2.2$ boundary shape, with similar global trends regarding discharge modifications as a function of lithium evaporation³⁰. A comparison of these boundary plasma shapes is shown in Figure 1, along with a schematic of two toroidally separated overhead LITHium EvapoRators (“LITER”) in NSTX. Note in particular that the centroid of LITER deposition was very close to the outer divertor strike point in the highly shaped plasma, whereas it was in the private flux region in the weakly shaped plasma. Here we present additional details of the progression of the lithium dose scan in the highly shaped discharge prototypical of NSTX-U, along with new SOLPS interpretive modeling to quantify the change in divertor recycling coefficient and cross-field transport rates.

II. Trends as a function of pre-discharge lithium

This was the first experiment in this particular campaign in which lithium was used; previous discharges used periodic boronization and inter-shot helium glow discharge cleaning. The pre-discharge lithium dose, along with the integral deposition, is shown as

a function of shot number in Figure 2. After obtaining ~ 10 reference discharges with both 5 and 6 MW neutral-beam injected (NBI) power, lithium was introduced for seven discharges at a dose ~ 150 mg. The next eight discharges used ~ 250 mg per discharge. The next six discharges varied the lithium dose between 250 and 500 mg each, with some alternation of high and low doses to assess hysteresis. The following eight discharges used ~ 450 mg per discharge, while the final nine discharges used ~ 500 -550 mg per discharge. The effects observed in this experiment depended mostly on the lithium dose between discharges, with a minor effect related to the integral dose.

Figure 3 shows the divertor D_α emission vs. time for select discharges during the lithium dose scan. The reference discharges were fairly well optimized in terms of pulse length (up to ~ 1 second) and discharge stored energy. Lithium was introduced before #132550, with doses as indicated in Figure 2. It can be seen that the baseline D_α was progressively reduced with increasing lithium dose. The external gas fueling was held constant until discharge #132566, and the NBI power was reduced to 4 MW for #132586. Generally the pulse lengths were longer with lithium conditioning once the fueling and NBI power was optimized. The longest pulses achieved were up to 1.2 s, e.g. #132557-132560.

Certain details of this lithium dose scan, e.g. the trends of D_α emission from the upper and lower divertors, as well as normalized energy confinement and midplane neutral pressure as a function of lithium dose for this high triangularity shape were presented previously³⁰. This paper builds on that previous work, with in-depth edge transport

modeling and recycling analysis; hence, a few details from the previous paper are summarized here for additional insights into the trends. Generally the D_α emission and neutral pressure decreased with increasing lithium dose, while normalized energy confinement increased. The trends with lithium dose in this high triangularity shape were similar to those observed during a Li dose scan with weaker shaping^{24, 25}, except that the rapid drop in lower divertor baseline D_α emission, which signifies the transition from high recycling to sheath limited divertor heat transport, occurred at a dose ~ 200 mg in the high triangularity dose scan, as compared to ~ 500 mg in the dose scan for the weakly shaped discharges. In addition the lower divertor baseline D_α emission dropped by 90% at the highest lithium dose in this lithium dose scan at high shaping, as compared to a $\sim 70\%$ drop observed during the scan at low shaping. Both of these differences are qualitatively consistent with the centroid of lithium deposition being closer to the outer strike point at high shaping than low shaping³⁰. Finally the trends in this experiment also agree semi-quantitatively with independent analysis of other discharges with 190 mg and 600 mg lithium dose in this discharge shape³¹, i.e. discharges that were not part of this systematic scan.

A comparison of the evolution of three discharges during the experiment is presented in Figure 4. These three discharges were used in the interpretive SOLPS modeling to quantify the reduction in divertor recycling coefficient and edge cross-field transport. Panel (a) displays plasma current I_p , panel (b) the NBI power P_{NBI} , panel (c) the line-averaged electron density from Thomson Scattering, panel (d) the normalized pressure

β_N , panel (e) the energy confinement time normalized to the ITER H97 L-mode scaling law³², panel (f) the radiated power in the core, and panel (g) the lower divertor D_α emission. The normalized pressure is defined by $\beta_N = \beta_t B_t a_m / I_p$, where β_t is the average plasma pressure normalized to the on-axis vacuum toroidal field: $\beta_t = 4\mu_0 W_{\text{MHD}} / (3V_p B_t^2)$. Also B_t is the toroidal field, a_m the minor radius, W_{MHD} the stored energy from equilibrium reconstructions, V_p the plasma volume, and μ_0 the permittivity of free space. The P_{NBI} was reduced from 6 \rightarrow 5 \rightarrow 4 MW with increasing lithium dose to keep the plasma below the global stability limit $\beta_N \leq 6$ (panels (b), (e)). The normalized confinement improved with increasing lithium dose (panel (e)). Note that the radiated power (panel (f)) was slowly increasing in the discharges with lithium conditioning; this is a commonly observed state when ELMs were eliminated (panel (g)) with lithium evaporation in NSTX²², thereby eliminating the periodic flushing of impurities. In addition the resulting profile changes changes neoclassical transport so that carbon and metallic impurities accumulated in the core, causing the temporal increased in radiated power.³³

III. SOLPS modeling

The SOLPS code³⁴ was used in interpretive analysis mode to quantify the changes in divertor recycling and cross-field transport; the procedure has been described in detail elsewhere for the discharges with moderate boundary shapes^{27, 29}. In brief, the divertor D_α peak emission is the primary constraint on the divertor target recycling coefficient, the divertor peak heat flux is the primary constraint on the separatrix location in the

reconstructed equilibrium (via power balance), and the density and temperature profiles serve to set the cross-field transport particle and thermal diffusivities.

A comparison between measured and simulated profiles is given in Figure 5 for the reference boronized discharge before lithium evaporation. The midplane n_e , T_e , and T_i profiles as a function of normalized poloidal flux ψ_N are obtained by ELM synchronization of multiple time slices to the last 50% of the ELM cycle. Note that $\psi_N = (\psi_0 - \psi(r))/(\psi_0 - \psi_{sep})$ with ψ_0 and ψ_{sep} being the poloidal flux at the magnetic axis and separatrix respectively. A comparison of the divertor profile data and simulations is plotted in physical space along the divertor target, from single time slices.

A few points are highlighted. First the T_i profile in the SOL is below the measured values. This is because the measurements in the SOL are representative of the fast ion population, as opposed to a thermal population. As a result, the T_e profile is used as a guideline to set the SOL cross-field ion heat transport. This comment applies to all three simulated timeslices in the succeeding paragraphs. In addition, the divertor D_α measurement saturated at a relatively low level; other measurements suggested the peak intensity was up to $\sim 10^{23}$ photons/m²/sec. Hence the simulated D_α was substantially [higher](#) than the measured value. The simulation used a divertor recycling coefficient $R_p = 0.995$, and a simulation using a value closer to unity would have been a somewhat more accurate representation. In addition the inner divertor D_α peak for $R < 0.3$ m from the simulation is physically on the center stack vertical section (Figure 1); due to the viewing

geometry, that peak is not measured by the 1-D CCD camera³⁵. This measurement limitation also applies to the simulations presented in Figures 6 and 7 also. Nonetheless, the baseline simulation was deemed sufficient as it represented a high recycling (but not “partially detached”³⁶) solution.

Figure 6 compares the measured profiles with simulations for the discharges with ~ 280 mg lithium dose. As can be seen by the plots, the simulated profiles and measured profiles are in good agreement except for the divertor D_α value, which is again underestimated. The divertor recycling coefficient $R_p = 0.94$, and probably should have been increased for a better match with data, but for the purpose of this study, the agreement was deemed acceptable.

Finally the measured and simulated profiles for the discharges with ~ 550mg lithium dose are shown in Figure 7. Overall the simulations and measured profiles are in very good agreement. These simulations used divertor recycling coefficient $R_p = 0.90$. Note that this divertor recycling coefficient is moderately higher than the $R_p=0.8-0.85$ inferred from UEDGE analysis of the individual 600mg discharge mentioned previously³¹.

In addition to quantifying the change in divertor recycling coefficient, the other primary purpose of the SOLPS simulations is to quantify the change in electron transport in the edge region near the separatrix. The simulations can only provide effective transport coefficients, i.e. separate diffusion and pinch terms cannot be accurately determined because this type of interpretive analysis is time independent.

Figure 8 shows the radial D_e and χ_e obtained from the SOLPS simulations to reproduce the measured profiles. The D_e decreased monotonically inside the separatrix, by factors of 10-30x, when comparing the reference and highest lithium dose discharge. On the other hand, the χ_e increased by up to 10x in the last 1-1.5cm nearest the separatrix, but decreased by 5x inside of that region. The near-separatrix region increase in thermal transport can be understood conceptually because a higher diffusivity is needed to drive the same cross-field heat flux at the reduced edge density obtained with lithium conditioning, e.g. see the profile changes shown elsewhere³⁰. The reduction in χ_e inside of that region was also observed with SOLPS analysis from the moderately shaped discharges; microstability analysis indicated a reduction in the drive for microtearing modes³⁷. Quantitatively the reduction in D_e and χ_e in these highly shaped discharges is very similar to those observed at moderate shaping^{25, 29}.

IV. Summary and Conclusions

In this paper we have used SOLPS modeling to quantify the reduction in divertor recycling and change in edge transport for low and high lithium dose, as compared to a reference boronized discharge without lithium, for a strongly shaped boundary NSTX H-mode discharge. The divertor recycling coefficient dropped from between 0.99 and 1.0, to ~ 0.9 for a 550mg lithium dose. In addition, both the particle and electron thermal diffusivity dropped substantially in a broad region 1-4 cm radially inward of the separatrix, although electron transport within 1cm of the separatrix increased substantially. Overall the results were very similar to a comparable lithium dose scan

conducted in moderately shaped discharges.

Overall these results bode well for lithium usage to enhance plasma performance and reduce recycling in NSTX-U³⁸, which is designed to use a highly shaped boundary plasma as in this study. Note that the lithium evaporators in NSTX-U will have the same geometry as in NSTX; thus, the centroid of the deposition will differ slightly from these experiments, owing to the larger center stack radius in NSTX-U. In addition, the fact that these plasmas responded in a similar manner to the dose scan in the moderately shaped discharges where the centroid of lithium deposition was 50 cm away from the outer strike point suggests that the positive effects of lithium coatings had saturated. Additional reduction in recycling, and possible further improvements in confinement, may require liquid lithium PFCs or greater wall coverage of solid PFCs, as observed e.g. in LTX¹³; such a flowing liquid lithium divertor upgrade is planned for NSTX-U.

Acknowledgements

This research was sponsored in part by U.S. Dept. of Energy under contracts DE-AC02-09CH11466, DE-AC05-00OR22725, DE-FC02-04ER54698, DE-FC02-99ER54512 and DE-AC52-07NA27344. We greatly acknowledge the contributions of the NSTX operations staff. The digital data for this paper can be found at: <http://arks.princeton.edu/ark:/88435/dsp01vx021h49j>.

Figure 1:

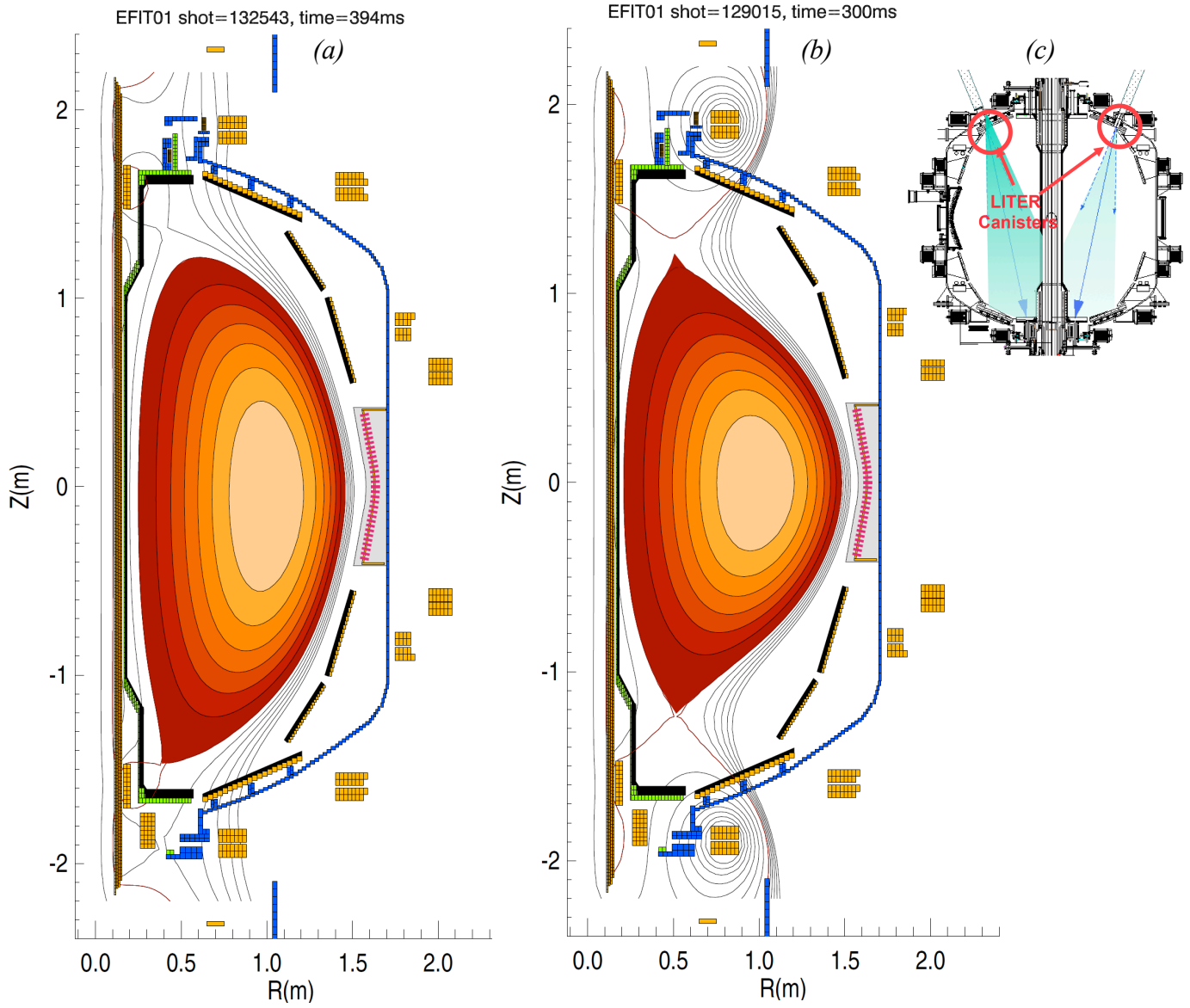


Figure 1: comparison of high and low δ shapes (a) and (b) with centroid of lithium evaporator deposition (c).

Figure 2:

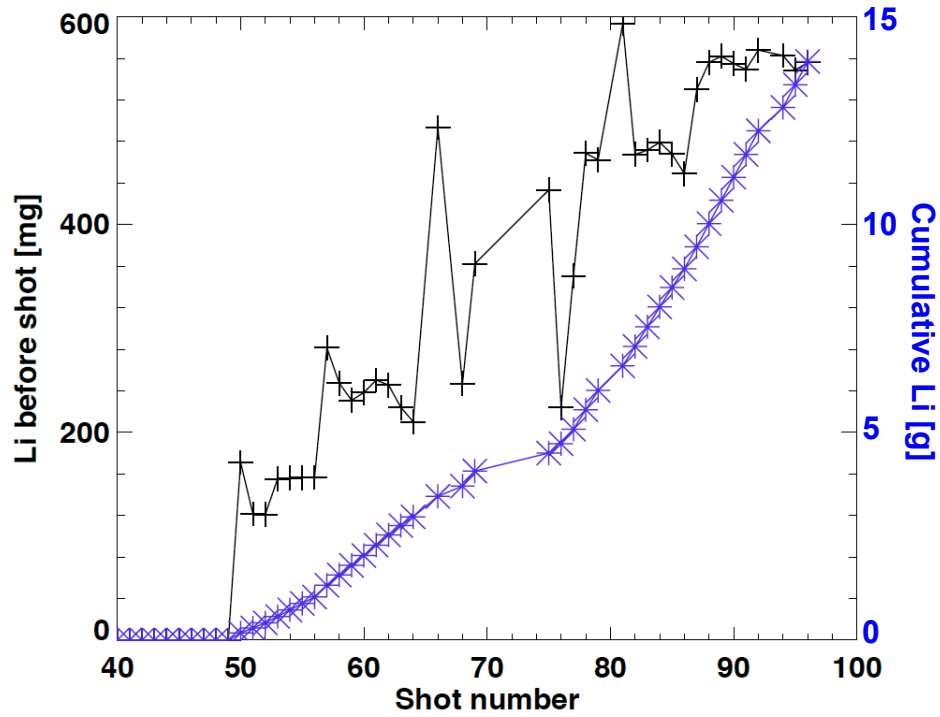


Figure 2: Lithium deposition before each discharge (black plus symbols) and cumulative (blue stars). The actual discharge number is obtained by adding 132500 to the x-axis.

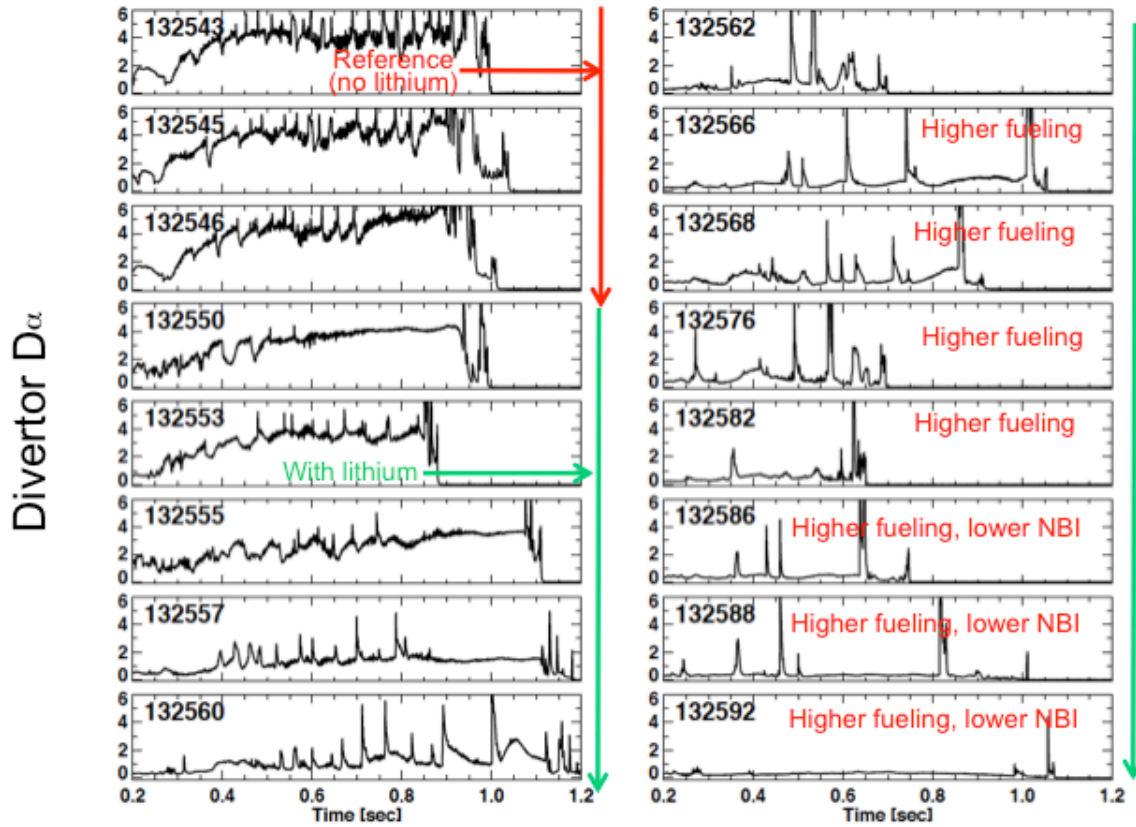


Figure 3: evolution of divertor D_{α} from selected discharges from the lithium evaporation scan. Gas fueling was held constant until #132566, and heating power was reduced starting with #132586.

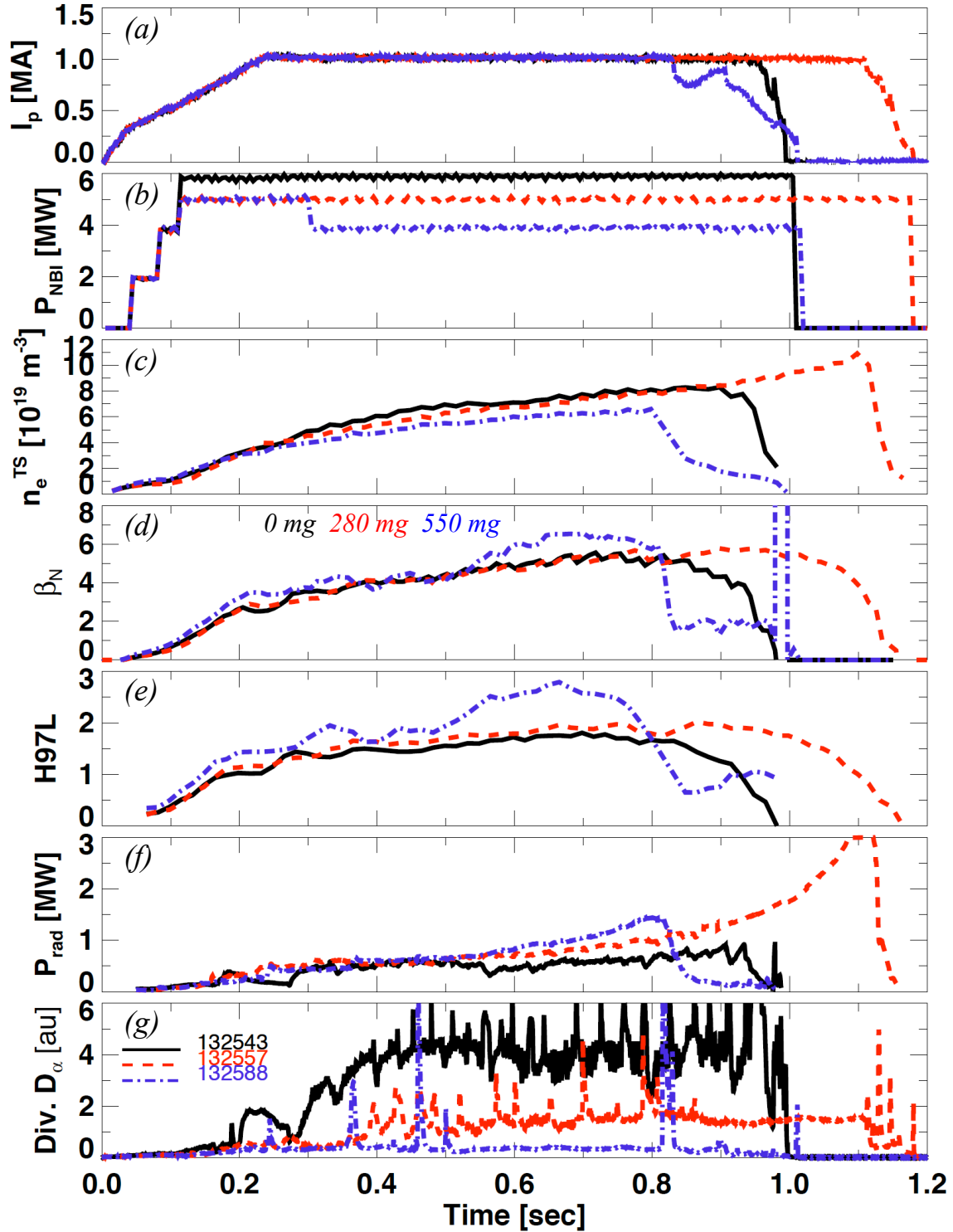


Figure 4: comparison of reference discharge (black) with intermediate (red) and high (blue) pre-discharge lithium evaporation. The NBI power was reduced modestly to stay below the global stability limit.

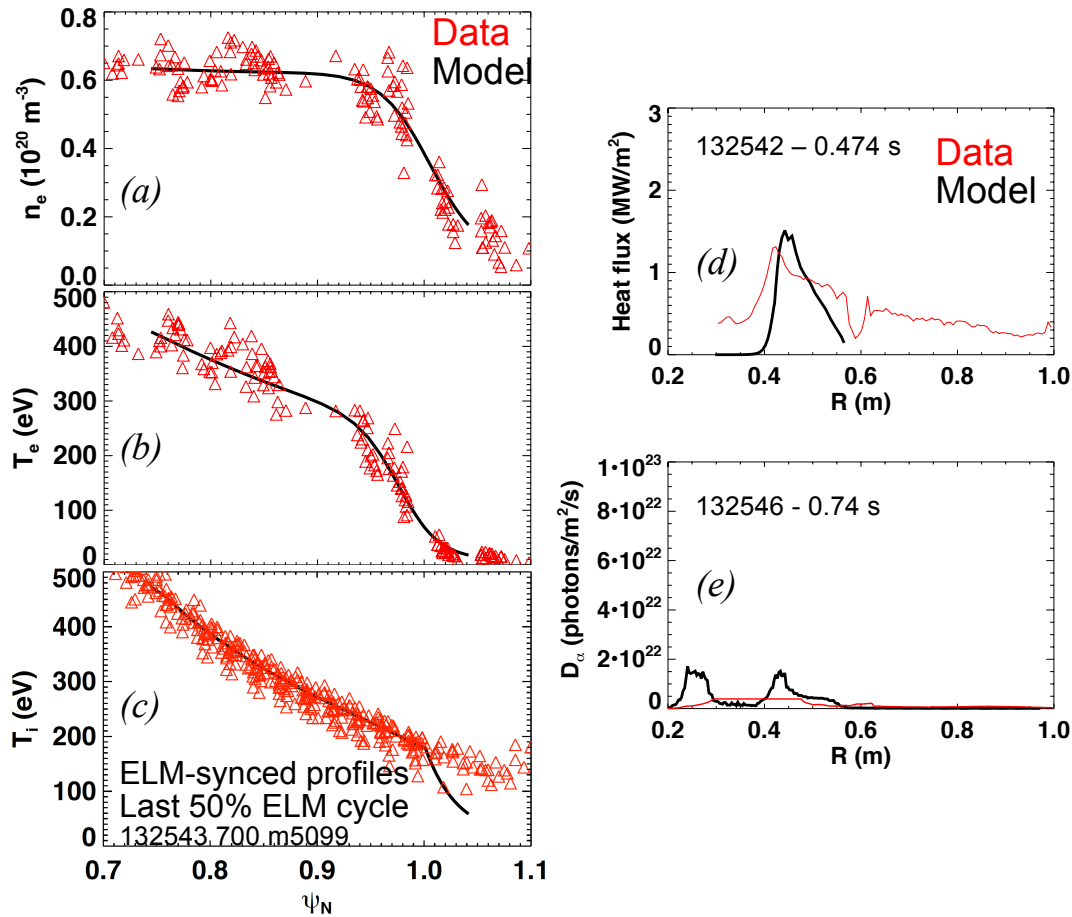


Figure 5: composite plasma profiles synced to the last 50% of the ELM cycle from reference boronized discharges with 6 MW NBI power: (a) electron density n_e , (b) electron temperature T_e , and (c) ion temperature T_i . The red symbols are data, and the solid black curve comes from SOLPS modeling. The lower divertor heat flux and peak D_α are shown in panels (d) and (e) respectively. The divertor D_α measurement saturated above 5×10^{21} photons/m²/s.

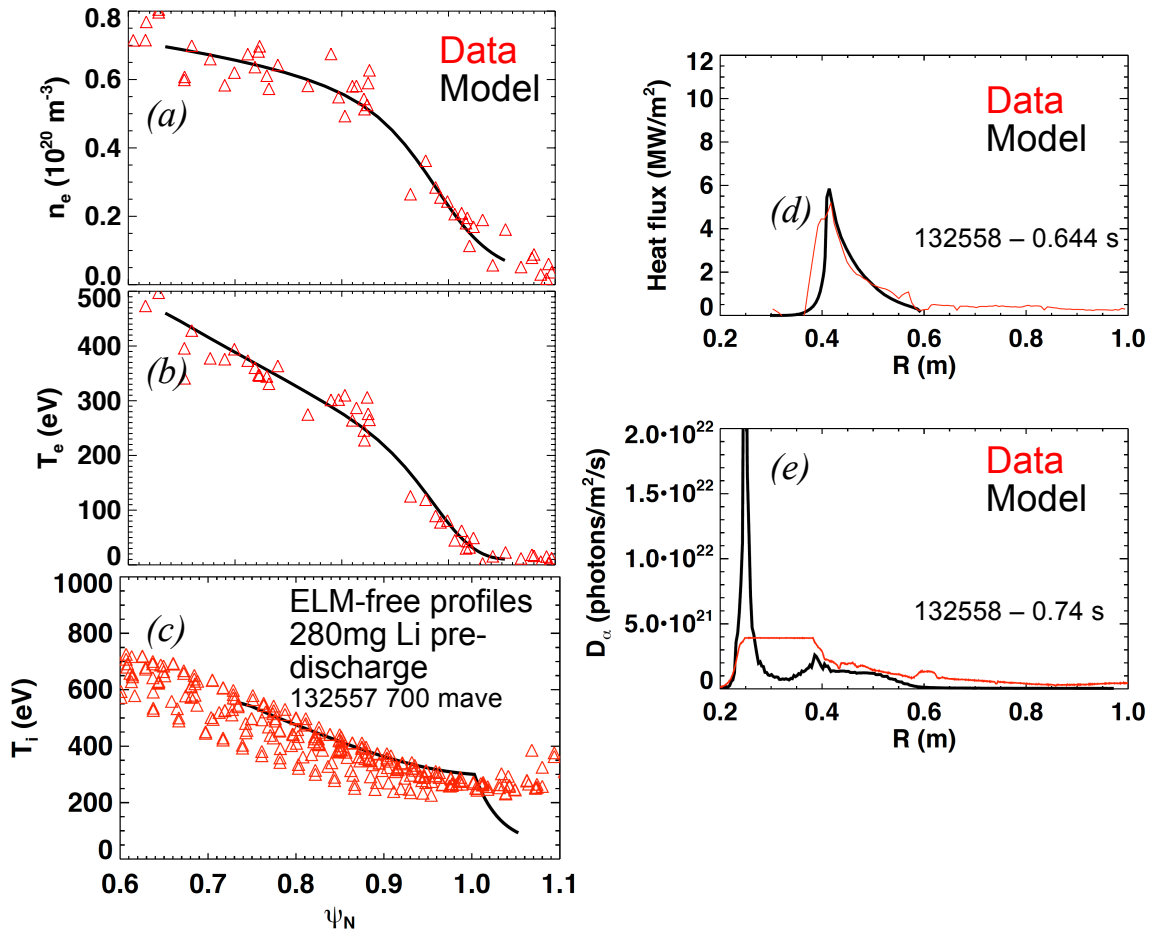


Figure 6: composite plasma during ELM-free phases from discharges with 5 MW NBI power and ~ 280 mg lithium dose: (a) n_e , (b) T_e and (c) T_i . The red symbols are data, and the solid black curve comes from SOLPS modeling. The lower divertor heat flux and peak D_α are shown in panels (d) and (e) respectively.

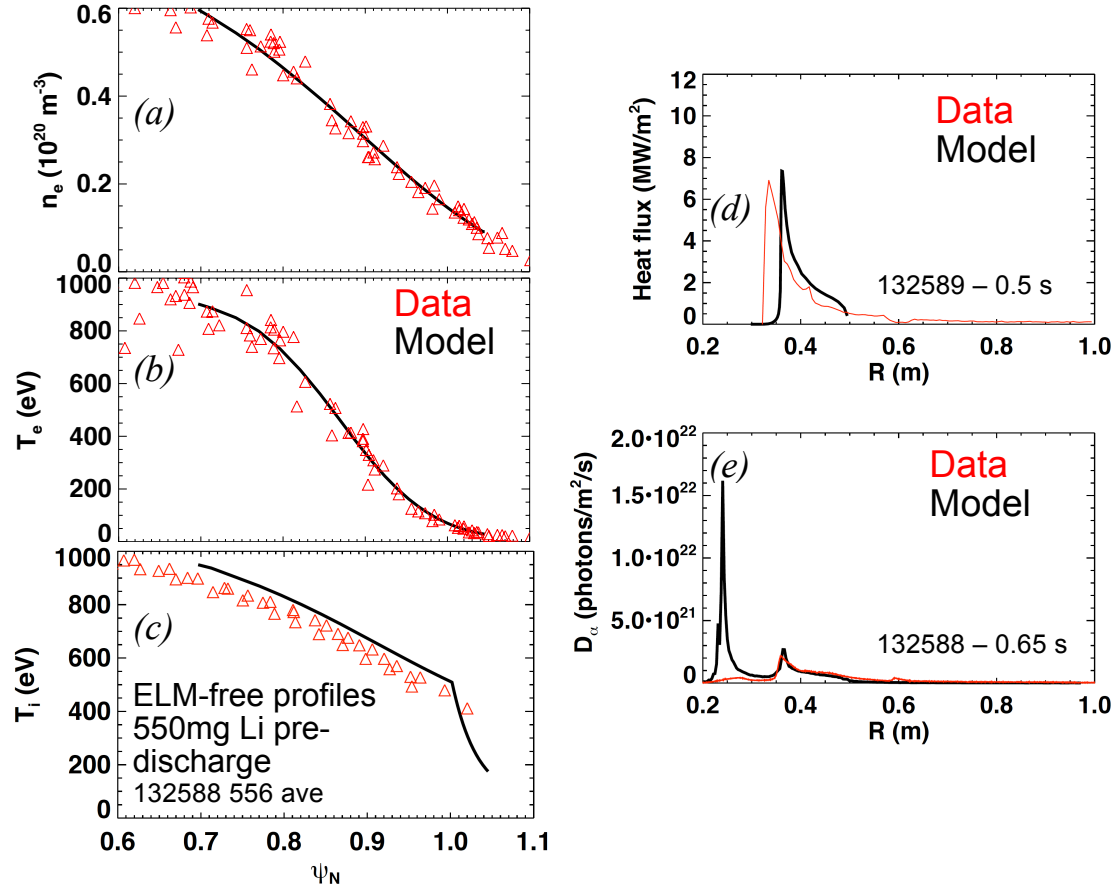


Figure 7: composite plasma profiles synced to the last 50% of the ELM cycle from reference boronized discharges with 6 MW NBI power: (a) electron density n_e , (b) electron temperature T_e , and (c) ion temperature T_i . The red symbols are data, and the solid black curve comes from SOLPS modeling. The lower divertor heat flux and peak D_α are shown in panels (d) and (e) respectively.

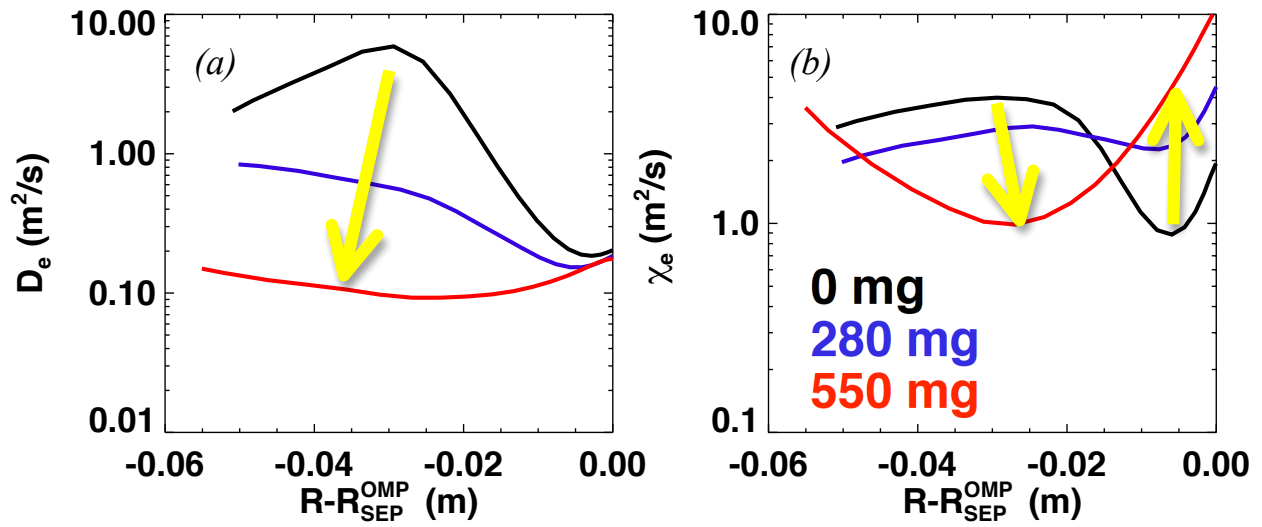


Figure. 8: (a) effective electron particle diffusivity D_e and (b) electron thermal conductivity χ_e vs. distance from the separatrix at the outer midplane. The yellow arrows indicate increasing levels of pre-discharge dose.

References

1. D. K. Mansfield *et al.*, *Phys Plasmas* **3** (1996) 1892.
2. Jackson G.L. *et al.*, *J Nucl Mater* **241** (1997) 655.
3. H. W. Kugel *et al.*, *J Nucl Mater* **363-365** (2007) 791.
4. D. K. Mansfield *et al.*, *Nucl Fusion* **41** (2001) 1823.
5. D. K. Mansfield *et al.*, *Fusion Eng Des* **85** (2010) 890.
6. T. H. Osborne *et al.*, *Nucl Fusion* **55** (2015) 063018.
7. J. S. Hu *et al.*, *Phys Rev Lett* **114** (2015) 055001.
8. D. K. Mansfield *et al.*, *Nucl Fusion* **53** (2013) 113023.
9. A. Bortolon *et al.*, *Nucl Fusion* **56** (2016) 056008.
10. M. A. Jaworski *et al.*, *Nucl Fusion* **53** (2013) 083032.
11. M. L. Apicella *et al.*, *Plasma Phys Control Fusion* **54** (2012) 035001.
12. R. Majeski *et al.*, *Bull Am Phys Soc* **56** (2011) 245.
13. J. C. Schmitt *et al.*, *Phys Plasmas* **22** (2015) 056112.
14. J. Ren *et al.*, *Physica Scripta* **T159** (2014) 014033.
15. J. S. Hu *et al.*, *Nucl Fusion* **56** (2016) 046011.
16. F. L. Tabarés, *Plasma Phys Control Fusion* **58** (2016) 014014.
17. F. L. Tabarés *et al.*, *Plasma Phys Control Fusion* **50** (2008) 124051.
18. H. W. Kugel *et al.*, *J Nucl Mater* **390-391** (2009) 1000.
19. H. W. Kugel *et al.*, *Phys Plasmas* **15** (2008) 056118.
20. H. W. Kugel *et al.*, *J Nucl Mater* **363-365** (2007) 791.
21. M. G. Bell *et al.*, *Plasma Phys Control Fusion* **51** (2009) 124054.
22. D. K. Mansfield *et al.*, *J Nucl Mater* **390-391** (2009) 764.
23. R. Maingi *et al.*, *Phys Rev Lett* **103** (2009) 075001.
24. D. P. Boyle *et al.*, *Plasma Phys Control Fusion* **53** (2011) 105011.
25. R. Maingi *et al.*, *Nucl Fusion* **52** (2012) 083001.
26. R. Maingi *et al.*, *Phys Rev Lett* **107** (2011) 145004.
27. J. M. Canik *et al.*, *J Nucl Mater* **415** (2011) S409.

28. D. Boyle *et al.*, *J Nucl Mater* **438** (2013) S979.
29. J. M. Canik *et al.*, *Phys Plasmas* **18** (2011) 056118.
30. R. Maingi *et al.*, *J Nucl Mater* **463** (2015) 1134.
31. V. A. Soukhanovskii *et al.*, *Proc 23rd Fusion Energy Conference, Daejon, Korea, 11-16 Oct 2010* (2010) paper EXD-P3-32.
32. S. M. Kaye, for the ITER Confinement and Transport Database Working Group, *Nucl Fusion* **37** (1997) 1303.
33. F. Scotti *et al.*, *Nucl Fusion* **53** (2013) 083001.
34. R. Schneider, *Contrib Plasma Phys* **46** (2006) 3.
35. V. A. Soukhanovskii *et al.*, *Rev Sci Instrum* **74** (2003) 2094.
36. C. S. Pitcher, and P. C. Stangeby, *Plasma Phys Control Fusion* **39** (1997) 779.
37. J. M. Canik *et al.*, *Nucl Fusion* **53** (2013) 113016.
38. J. E. Menard *et al.*, *Nucl Fusion* **52** (2012) 083015.

Princeton Plasma Physics Laboratory Office of Reports and Publications

Managed by
Princeton University

under contract with the
U.S. Department of Energy
(DE-AC02-09CH11466)

P.O. Box 451, Princeton, NJ 08543
Phone: 609-243-2245
Fax: 609-243-2751

E-mail: publications@pppl.gov

Website: <http://www.pppl.gov>